Topology Optimization of a Surface Permanent Magnet Motor with High Torque Density

Shogo Hayashi[1], Manabu Yatsurugi[2], Yoshihisa Kubota[2], Shingo Soma[2], and Hajime Igarashi[1]

[1]Graduate School of Information Science and Technology, Hokkaido University, Sapporo 060-0814, Japan
[2]Honda R&D Co., Ltd. Automobile R&D Center, Tochigi 321-3393, Japan

This paper introduces a topology optimization method for a surface permanent magnet (SPM) motor with high torque density suitable for air mobility. The proposed method can be used to determine the material distribution and magnetization direction in PMs to maximize the torque density at a constant current. The torque performance of the optimized motor is superior to that of a conventional motor with a Halbach array, whose magnetization varies linearly along the circumferential direction. The novel optimized motor has a triangular magnetic material on the rotor surface and an air region inside the rotor.

***Index Terms*— Air mobility, Halbach array, surface permanent magnet motor, topology optimization**

I. Introduction

In recent years, air mobility has attracted considerable attention [1], [2]. Surface permanent magnet (SPM) motors, shown in Fig. 1, are used in air mobility propulsion systems because of their high output per unit mass. Halbach magnet arrays are widely used in SPM motors because of their high output power [3]. To reduce the mass of air mobility propulsion systems, the performance of SPM motors must be improved.
In addition, the remarkable progress in three-dimensional metal printing technology is expected to facilitate the fabrication of magnets with a continuous magnetization direction [4]. It may be possible to realize an SPM motor, whose performance is better than that of a Halbach motor, using permanent magnets (PMs) with a continuous magnetization direction and other materials. However, optimizing the magnetization direction by trial and error is a difficult process. Therefore, a method is required to optimize the magnetization direction and shape of a PM and magnetic core simultaneously.

In this paper, we propose a multi-material topology optimization method that determines the distribution of iron, air, and PMs as well as the magnetization direction. The novelty

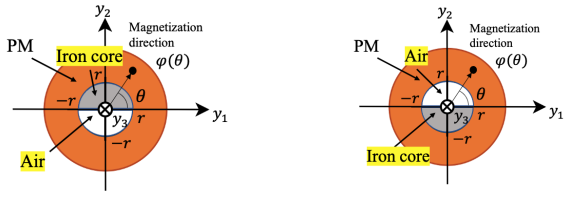

(a) $y_3 \le 0$ (b) $y_3 > 0$

Fig. 3. State space for proposed method II

of this work is that not only the material distribution but also the magnetization distribution are optimized, which will be shown to be very effective for optimization of SPM motors for air mobility. The proposed method was applied to optimize the design of an SPM motor with high torque density suitable for an air mobility propulsion system. The proposed method was applied to develop a novel-shaped SPM motor, whose torque density was higher than that of the reference Halbach motor.

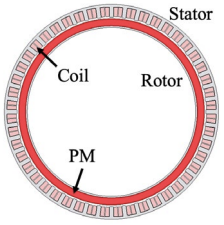

Fig. 1. Structure SPM motor

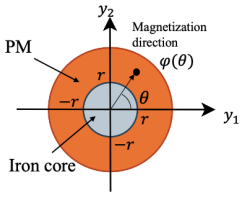

Fig. 2. State space for proposed method I

II. Proposed Method

A. Conventional Topology Optimization

In this study, we employed the NGnet method owing to its high searchability and versatility. In this method, Gaussian basis functions are placed in the design region, and the material distribution is determined from the shape function, which is defined as:

$$y(\boldsymbol{x}, \boldsymbol{w}) = \sum_{i=1}^{N} w_i b_i(\boldsymbol{x}) \tag{1}$$

where, $\boldsymbol{w}_i$ is the weighting coefficient, $\boldsymbol{x}$ is the position vector, N is the number of Gaussian basis functions, and $b_i(\boldsymbol{x})$ is the normalized Gaussian basis function, which is defined as:

$$b_i(\boldsymbol{x}) = \frac{G_i(\boldsymbol{x})}{\Sigma_{k=1}^{N} G_k(\boldsymbol{x})} \tag{2}$$

$$G_k(\boldsymbol{x}) = \frac{1}{2\pi\sigma^2} \exp\left[-\frac{\|\boldsymbol{x} - \boldsymbol{\mu}_k\|^2}{2\sigma^2}\right] \tag{3}$$

where $\boldsymbol{\mu}_k$ and σ^2 are the centers of the k-th Gaussian basis and variance, respectively. The material attribute v_e of the finite element e is determined from

$$v_e \leftarrow \begin{cases} \text{air}, & y < 0 \\ \text{iron}, & y \ge 0 \end{cases} \tag{4}$$

Material distribution depends on $\boldsymbol{w}$, which minimizes the cost function, implying that topology optimization is reduced to parameter optimization with respect to $\boldsymbol{w}$.

B. Proposed Method to Determine Magnetization Direction

Because the shape function y of NGnet is represented by a weighted sum of normalized Gaussian functions with a smooth distribution, it can be to determine magnetization directions with a smooth distribution suitable for manufacturing. Representing three or more materials and the magnetization directions of PMs using a single shape function is a considerable challenge, and therefore, multiple shape functions are used.

In this paper, we propose two methods; in addition to optimization of the magnetization direction of PMs, proposed method I determines the distribution of iron and PMs, and proposed method II determines the distributions of iron, PMs and the air region.

In proposed method I, two shape functions $y_1(\boldsymbol{x}, \boldsymbol{w}_1)$ and $y_2(\boldsymbol{x}, \boldsymbol{w}_2)$ are distributed over the design region with two weighting vectors $\boldsymbol{w_1}$ and $\boldsymbol{w}_2$ of the NGnet. The material and magnetization directions in the design domain are determined using a pair of shape functions, as shown in Fig. 2; in Fig. 2, r is the radius of the circle that serves as the boundary between the material iron and PM, and φ is the magnetization direction with respect to the radial direction and is determined as:

$$\varphi = \frac{1}{2}\left|\tan^{-1}\left(\frac{y_2}{y_1}\right)\right| \tag{4}$$

if $\sqrt{y_1^2 + y_2^2} \geq r$. For given $\boldsymbol{w_1}$ and $\boldsymbol{w_2}$, we can determine y_1 and y_2 in a finite element, and these two shape functions are then used to identify the material of the element (iron or magnet) and magnetization of the magnet as illustrated in Fig. 2. Tani *et al.* [11] simultaneously optimized the magnetization direction and material distribution based on the state space, which was different from that shown in Fig. 2.

Because it is necessary to reduce the mass of PM motors for air mobility, an air region should also be introduced. Proposed method II introduces an additional shape function y_3 $(\boldsymbol{x}, \boldsymbol{w}_3)$ in addition to y_1 and y_2. Different state distributions exist depending on y_3 as shown in Fig. 3. Introduction of y_3 allows us to well represent the material transition from PM to air or iron. Note that we need $3N$ basis functions b_i for the three dimensional state space spanned by y_1, y_2 and y_3 in the rotor.

III. Optimization Results

A. Optimization Problem

The SPM motor model and arrangement of the Gaussian functions are shown in Fig. 4, and their specifications are summarized in Table I. In this study, the rotor shape was optimized using proposed methods I and II, in which the shape of the tooth tip was also optimized in terms of the weighting coefficient w_t. The numbers of design variables for proposed methods I and II, $\boldsymbol{w} = \{\boldsymbol{w}_1, \boldsymbol{w}_2, \boldsymbol{w}_t\}$ and $\{\boldsymbol{w}_1, \boldsymbol{w}_2, \boldsymbol{w}_3, \boldsymbol{w}_t\}$, were 44 and 60, respectively. In the optimization process, we maximized the average torque density T_{avg} [Nm/kg] at $I_{\max} \leqq$ 250 Arms as follows:

$$\text{Maximize} \quad T_{avg}(\boldsymbol{w_{all}}) \tag{5}$$

We determined w for the NGnet using the covariance matrix adaptation evolution strategy (CMA-ES) [12], which is a population-based stochastic algorithm. In the CMA-ES, the number of individuals required for the global search increases only in O($logN$), whereas that for the genetic algorithm typically increases in O(N), where N represents the number of optimization variables. In the CMA-ES, individuals are generated according to the mean vector and covariance matrix, which are adaptively changed during the optimization. A flow diagram of the hybrid optimization, which ends at

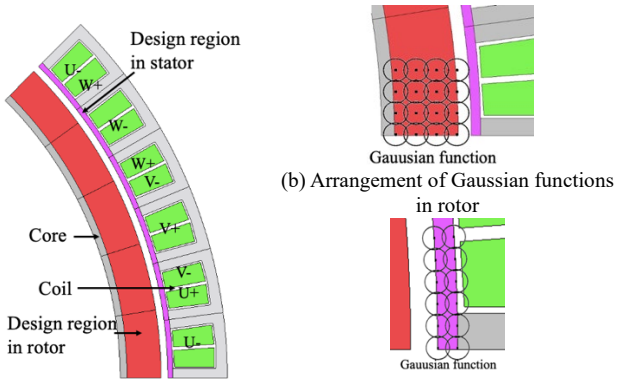

(a) Analysis model (b) Arrangement of Gaussian functions in rotor (c) Arrangement of Gaussian functions in stator

Fig. 4. Analysis model

TABLE I
MOTOR SPECIFICATIONS

Phases and poles	3 phases, 40 poles
Stator outer diameter [mm]	($\Phi \leqq 350$)
Thickness [mm]	($t \leqq 85$)
Air gap [mm]	2
Coil Turns	5
Number of stator slot	48
Residual flux density [T]	1.4
Electromagnetic steel sheets	Permendur

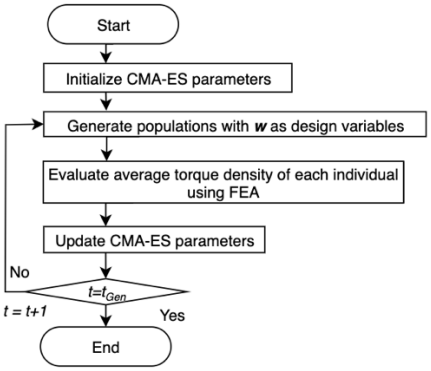

Fig. 5. Flow diagram of optimization

TABLE II
SETTING OF THE CMA-ES

Number of Generation	100
Size of population	64
Number of genes: Proposed method I	44
Number of genes: Proposed method II	60
Initial mean vector	0.00
Initial variance	0.16

generation t_{gen}, is shown in Fig. 5. The optimization settings are summarized in Table II. For the other parameters, we used the values recommended by Hansen *et al.* [12].

B. Optimization Results

The optimization results were compared with those of the Halbach motor shown in Fig. 6; in Fig. 6, the magnetization direction is constant in the radial direction and varies linearly along the circumferential direction. The characteristics of the motor obtained by optimization are expressed as numerical values normalized by those of the Halbach motor.

Fig. 7 and 8 show the magnetization direction and magnetic flux lines of the optimized motor determined using proposed method I ($r = 0$ and 0.4, respectively), respectively, and Fig. 9 shows the same parameters derived using proposed method II ($r = 0.4$). As shown in Fig. 7, proposed method I ($r = 0$) considers only the magnetization distribution. By contrast, the results shown in Fig. 8 are derived using the same method ($r = 0.4$) by considering the distribution of the core and PM in addition to the magnetization. The results shown in Fig. 9 are derived using proposed method II ($r = 0.4$) by considering the distribution of the air region. The torque waveforms of the reference and optimized motors are shown in Fig. 10. The average torque density, torque, and mass are listed in Table III.

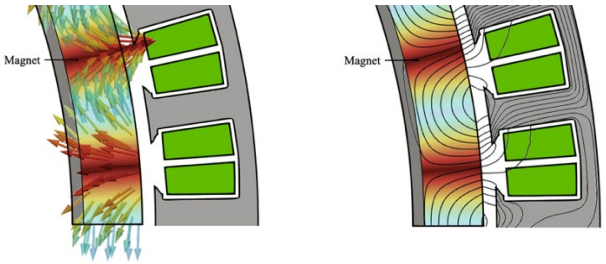

(a) Magnetization direction (b) Flux line

Fig. 6. Reference motor

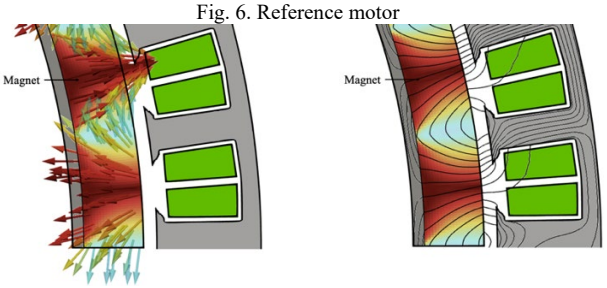

(a) Magnetization direction (b) Flux line

Fig. 7. optimized motor by proposed method I (r=0.0)

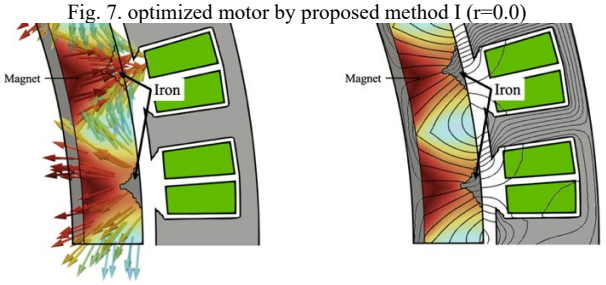

(a) Magnetization direction (b) Flux line

Fig. 8. optimized motor by proposed method I (r=0.4)

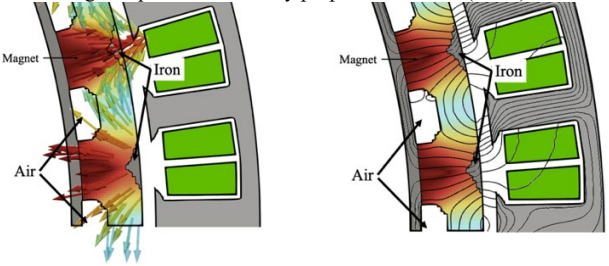

(a) Magnetization direction (b) Flux line

Fig. 9. optimized motor by proposed method II (r=0.4)

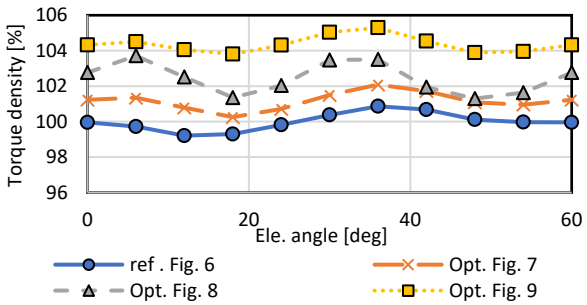

Fig. 10. Torque density waveformes of reference and optimized motors

TABLE III
CHARACTERISTICS OF THE REFERENCE MODEL AND OPTIMIZED MOTORS

	Ave. torque density [%]	Ave. torque [%]	Mass [%]
Ref.	100.0	100.0	100.0
Opt. (a)	101.2	101.1	99.93
Opt. (b)	102.4	102.1	99.73
Opt. (c)	104.4	98.15	94.04

The features of the optimized motor include: (i) the distribution of magnetization direction changing into radial direction, (ii) a wedge-shaped iron above the pole near the rotor surface, and (iii) a trapezoidal air region with rounded corners between the poles.

Next, we discuss the characteristics of the optimized motors. Both Fig. 6 and 7 present results obtained for a Halbach motor, although the magnetization distributions shown in these two figures are different. A Halbach array was obtained via random magnetization using the proposed method. The optimized magnetization direction changed to the radial direction, which reduced the path of the magnetic flux compared to that in the reference Halbach motor and decreased the magnetic resistance. Consequently, the average torque density was improved by 1.2 %.For the optimized motors shown in Fig. 7 and 8, the magnetization distributions are almost the same; however, the motor depicted in Fig. 8 has a wedge-shaped iron on the rotor surface. The average torque density of the motor shown in Fig. 7 is 1.2 % higher than that of the motor shown in Fig. 8. Further, Fig. 8(b) reveals that the magnetic flux is concentrated in iron, which decreases the magnetic resistance.

Finally, both the optimized motors shown in Fig. 8 and 9 have a wedge-shaped iron on their rotor surfaces. However, Fig. 9 exhibits a trapezoidal air region with rounded corners between the poles. The average torque values in Table III indicate that the geometry shown in Fig. 9 has a superior torque density, which is important for air mobility.

C. *Discretization of Magnetization Direction*

In the previous subsection, we discussed motors in which the magnetization direction of the PM is assumed to be continuously distributed. However, manufacturing SPM motors with continuous magnetization directions is a challenging task. Therefore, we considered discretized magnetization directions from the viewpoint of manufacturability. The magnetization directions of the PMs were discretized into the three nearest magnetization directions: 0°, 45°, and 90°. The discretized magnetization directions and flux lines of the reference motor shown in Fig. 6 and 9 are depicted in Fig. 11 and 12, respectively. The corresponding waveforms are shown in Fig. 13, and their characteristics are summarized in Table IV. Upon discretization, the magnetic flux lines in the PM become angular, and the magnetic resistance increases, which deteriorate the torque characteristics of both the shapes. Although discretization deteriorated the average torque by 1.5 %, the performance of the discretized optimized motor remained superior to that of the reference motor.

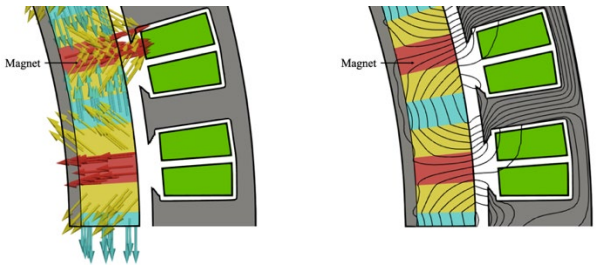

(a) Magnetization direction (b) Flux line

Fig. 11. Discretized reference motor

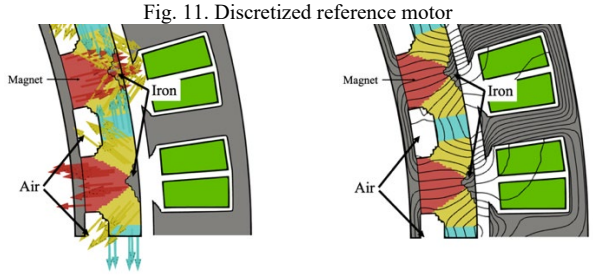

(a) Magnetization direction (b) Flux line

Fig. 12. Discretized optimized motor

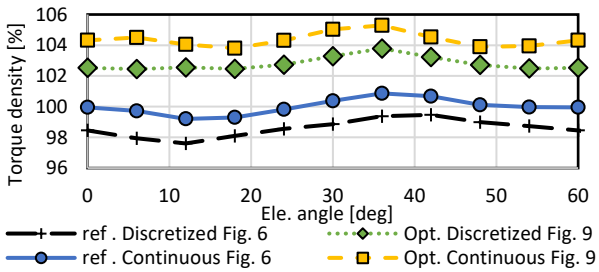

Fig. 13. Torque density waveformes of discretized reference and optimized motors

T TABLE IV
CHARACTERISTICS OF THE DISCRETIZED REFERENCE AND OPTIMIZED MOTORS

	Ave. torque density[%]	Ave. torque [%]	Mass [%]
Ref.	98.61	98.61	100.0
Opt. (c)	102.8	96.70	94.04

IV. Conclusion

In this paper, we proposed a topology optimization method to determine multiple material distributions and magnetization direction. Optimization using the proposed method yielded three novel features: (i) PMs whose magnetization direction changed to circumferential and radial directions, (ii) a wedge-shaped iron above the pole near the rotor surface, and (iii) a trapezoidal air region with rounded corners between the poles. These three features collectively increased the average torque density, which was found to be higher than that of a conventional Halbach motor.

Acknowledgment

This work was supported in part by a Grant-in-Aid for Scientific Research (KAKENHI) awarded by the Japanese Society for the Promotion of Science under Grant 21H01301.

References

[1] N. Polaczyk N.E.Trombino, P.Wei, M.Mitici, “A review of current technology and research in urban on-demand air mobility applications” in *Proc. 8th Biennial Auton. VTOL Tech Meeting 6th Annu. Electr. VTOL Symp.*, Jan. 2019, pp. 333–343.

[2] J. A. Swanke and T. M. Jahns, “No. 22260632,” *IEEE Trans. Transp. Electrif.*, vol. 8, no. 4, Dec., 4523–4533, 2022, DOI: 10.1109/TTE.2022.3183933.

[3] K. Atallah and D. Howe, “The application of Halbach cylinders to brush-less ac servo motors,” *IEEE Trans. Magn.*, vol. 34, no. 4, pp. 2060–2062, Jul. 1998, DOI: 10.1109/20.706795.

[4] C. Huber *et al.*, “3D print of polymer bonded rare-earth mag- nets, and 3D magnetic field scanning with an end-user 3D printer,” *Appl. Phys. Lett.*, vol. 109, no. 16, Oct., Art. no. 162401, 2016, DOI: 10.1063/1.4964856.

[5] J. Lee and S. Wang, “Topological shape optimization of permanent magnet in voice coil motor using level set method,” *IEEE Trans. Magn.*, vol. 48, no. 2, pp. 931–934, Feb. 2012, DOI: 10.1109/TMAG.2011.2173922.

[6] Y. Yamashita and Y. Okamoto, “Design optimization of synchronous reluctance motor for reducing iron loss and improving torque characteristics using topology optimization based on the level-set method,” *IEEE Trans. Magn.*, vol. 56, no. 3, pp. 1–4, Mar. 2020.

[7] F. Guo and I. P. Brown, “Simultaneous magnetic and structural topology optimization of synchronous reluctance machine rotors,” *IEEE Trans. Magn.*, vol. 56, no. 10, pp. 1–12, Oct. 2020, DOI: 10.1109/TMAG.2020.3014289.

[8] T. Sato, K. Watanabe, H. Igarashi., “‘Multimaterial topology optimization of electric machines based on normalized Gaussian network,’ *IEEE Trains*,” *Magn.,* vol. 51, no. 3, Mar., Art. no. 7202604, 2015.

[9] S. Hayashi, Y. Kubota, S. Soma, M. Ohtani, H. Igarashi, ”Topology optimization of permanent magnet synchronous motor considering the control system,” *IEEE Trans. Magn.*, vol. 58, no. 9, Sep., 1–5, 2022, DOI: 10.1109/TMAG.2022.3172718.

[10] S. Hayashi and H. Igarashi, “Parameter-topology hybrid optimization of electric motor with multiple permanent magnets,” *Int. J. Appl. Electromagn. Mech*., vol. 71, pp. S245–S255, 2023.

[11] K. Tani, Y. Kida, T. Yamada, “A study on simultaneous optimization of material distribution and orientation direction of magnets in permanent magnet motors (in Japanese)”, Technical Report of IEE Japan, SA-22-092, RM-22-095, 2022.

[12] N. Hansen, D.V. Arnold, A.Auger, *Evolution Strategies; Handbook of Computational Intelligence*, J. Kacprzyk and W. Pedrycz, Eds. Springer, pp. 871–898, 2015.